Journal of Molecular Structure 1248 (2022) 131435

Contents lists available at ScienceDirect

Journal of Molecular Structure

journal homepage: www.elsevier.com/locate/molstr

Insight into structural description of novel 1,4-Diacetyl-3,6-bis(phenylmethyl)-2,5-piperazinedione: synthesis, NMR, IR, Raman, X-ray, Hirshfeld surface, DFT and docking on breast cancer resistance protein

Koffi Sénam Etsè[a,*], Guillermo Zaragoza[b]

[a] Laboratory of Medicinal Chemistry, Center for Interdisciplinary Research on Medicines (CIRM), University of Liège, Quartier Hôpital B36 Av. Hippocrate 15 B-4000 Liège, Belgium

[b] Unidade de Difracción de Raios X, RIAIDT, Universidade de Santiago de Compostela, Campus VIDA, 15782 Santiago de Compostela, Spain

ARTICLE INFO

Article history:
Received 30 July 2021
Revised 30 August 2021
Accepted 1 September 2021

Keywords:
diketopiperazine
crystal structure
puckering parameters
DFT calculations, Hirshfeld surface, breast cancer resistance protein

ABSTRACT

In this work, novel 1,4-diacetyl-3,6-bis(phenylmethyl)-2,5-piperazinedione (**2**) is prepared exclusively as the (*R,S*)-stereoisomer evidenced and confirmed by X-ray diffraction analysis. In addition, spectroscopic (NMR, IR, Raman) analyses were used to characterize the new compound. **2** crystallizes in the *Pbca* orthorhombic space group, with a symmetry center located at the centroid of the diketopiperazine ring. The structure of **2** is compact with the two phenyl rings folded over and under the diketopiperazine ring, conferring thereby a unique *S* shape to the molecule. The crystal structure is stabilized by intramolecular interactions, whereas the crystal packing is stabilized by intermolecular H-bond and C–H···π interactions. The different intermolecular interactions were confirmed using Hirshfeld surface analysis and molecular fingerprint. Molecular 2D fingerprint that quantify the different interactions highlights that H···H (58.2%), H···O/O···H (24.8%) and C···H/H···C (14.2%) account for 97.2% of all contacts. The topology of the interaction energy in the crystal structure is obtained and described. The Cremer and Pople puckering parameters indicate that the diketopiperazine ring adopts a flattened chair conformation with $\Theta = 0.00$ ° and $Q = 0.2233$ (11) Å. Moreover, a computational investigation revealed that the optimized structure of **2** using DFT calculation shows excellent agreement with the experimental data. As potential pharmacological active molecule, the molecular docking on breast cancer resistance protein (BCRP) reveals that **2** could interacts with the binding domain residues Phe728, Tyr949, Ser975 and Val978 and could be consider as promising BCRP inhibitor.

1. Introduction

Diketopiperazines (DKPs) are a class of compounds displaying a wide range of biological activities [1–2] as antibacterial [3–4], antifungal [5,6], antitumoral [7–9] and antiviral agents [10,11]. Some DKP derivatives exhibit radical-scavenging and antioxidant activities [12,13]. 3,6-disubstituted 2,5-diketopiperazines, whether natural or synthetic, are the most abundant and have received enormous attention because of their structure related to cyclodipeptides [14–17]. Unlike linear (di)peptides, constraining the nitrogen atoms of an α-amino amide into a DKP ring modify physical properties, reduces susceptibility to metabolic amide bond cleavage reactions and reduces conformational mobility. As a result of the change in structural and physical characteristics, DKPs can confer more drug-like properties to molecules and enhance favorable interactions with biological macromolecules [15].

The symmetrical cyclic dipeptide (L-Phe-L-Phe) with two phenylalanine residues was originally isolated from *Penicillium nigricans* [18] and then from a marine mangrove endophytic fungus [19]. *cyclo*(L-Phe-L-Phe) also occurs in a variety of beverages and foods such as beef, cheddar cheese, cocoa, white wine, yeast extract [20] and chicken essence [21]. It has been shown to exhibit good anthelmintic activity against *Hymenolepis nana* and *Schistosoma mansoni* [22] and antidepressant and antidementia effects in mice [23] as well as moderate antioxidant efficiencies against the standard antioxidants ascorbic acid (natural) and butylated hydroxyanisole (a synthetic ingredient used in food, cosmetics, and medicine) [13].

Tryprostatin-A (TPS-A; ((3S,8aS)-3-[[6-methoxy-2-(3-methylbut-2-enyl)-1Hindol-3-yl] methyl]-2,3,6,7,8,8a-hexahydropyrrolo[1,2-

* Corresponding author.
E-mail address: ks.etse@uliege.be (K.S. Etsè).

https://doi.org/10.1016/j.molstruc.2021.131435
0022-2860/

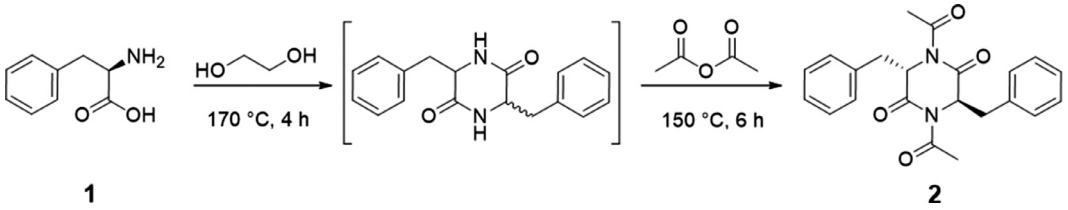

Fig. 1. Synthesis of 1,4-diacetyl-3,6-bis(phenylmethyl)-2,5-piperazinedione (**2**).

a]pyrazine-1,4-dione)) is a DKP derivative with (*cyclo*-L-Trp-L-Pro) backbone. TPS-A is well known as one of the most efficient and specific inhibitors of breast cancer resistance protein (BCRP) [24]. Indeed, after drug administration, ATP-binding cassette proteins are produced in organs for absorption, distribution and elimination of drugs. In serious pathologies like cancers, I was shown that resistance of cancer cells to anticancer drugs comes from the increasing production of ATP-binding cassette proteins [25]. It is therefore suggested that modulation of the activity of these proteins could be beneficial in resistant cancer therapy. BCRP is one of ATP-binding cassette proteins. Recently, Fani et al. described a new series of DKP derivatives as simultaneous effective inhibitors of $\alpha\beta$-tubulin and BCRP proteins [26]. Although most of cyclic dipeptides with biochemical properties have been isolated from natural organisms ranging from bacteria to humans [8,12,27–29], others [13,30] have been synthesized chemically through a systematic structure−activity analysis, by taking inspiration from the structure of lead compounds. The structure of cyclodipeptides could therefore highly variable, ranging from the simplest, unmodified cyclic dipeptides [12,31] to heavily modified skeletons [28,32].

The conformations of various DKPs have been experimentally investigated both in solution and the solid state, as well as by computational methods [33–37]. It turned out that the molecular conformation of cyclic dipeptides could depend on the relative configuration of the two amino acids, the nature of their residue, and *N*-acetylation or methylation [33–36]. Furthermore, intra- and intermolecular hydrogen bondings could be the major contributors but other intermolecular interactions, such as π-stacking and C=O/C=O dipole packing forces [35,36] could also contribute substantially to the crystal structure conformation. In this line, Adler-Abramovich and coworkers showed that in the case of *cyclo*(L-Phe-L-Phe), ordered vertically aligned nanotubes material obtaining could arise from stacking interaction between aromatic moieties providing the energetic contribution needed for the formation of such well-ordered structures [38].

As part of our studies on development of new diketopiperazine derivatives and the molecular structure determination, we became interested in *N,N*'-diacetyl-cyclodiphenylalanine (**2**) (Fig. 1). This work aims to investigate the effects of the acetyl groups and to determine if the starting residues chirality affects the structural conformation of the cyclopeptide **2** [39]. According to literature, this goal could be achieved by the full characterization and the determination of the molecular structure of **2** [40,41]. Furthermore, the experimental results will be compared to similar reported structures that could provide a critical comparison analysis of the data. The scope of this work will finally expand to the biological potentiality of this new DKP. This work report therefore on the synthesis and the full characterization of 1,4-diacetyl-3,6-bis(phenylmethyl)-2,5-piperazinedione by NMR, infrared and Raman spectroscopy. Furthermore, full description of the molecular structure obtained by X-ray diffraction analysis and interactions stabilizing the crystal structure of this DKP are described. Particular attention was paid to analyze the conformation adopted by the diketopiperazine ring thanks to Cremer and Pople parameters. The conformation adopted by the new DKP was also compared to the optimized structure obtained using DFT calculation. Finally, as potential drug candidate, molecular docking study on breast cancer resistance protein was performed.

2. Materials and methods

All solvents (ethylene glycol, dichloromethane, petroleum ether) and reagents (L-phenylalanine and acetic anhydride) were purchased from TCI or Sigma-Aldrich. Solvents for chromatography were used as received without further purification. All reactions were monitored and analyzed by TLC using Macherey-Nagel 0.2 mm pre-coated Alugram® N/UV254 silica gel or alumina gel plates. Column chromatography was conducted using 60 Å, 70–230 mesh, 63–200 μm silica gel supplied by Grace Davison or Sigma-Aldrich. Petroleum ether refers to the fraction boiling at 40–60 °C. Analyses by ^{1}H and ^{13}C NMR spectroscopy were achieved at 298 K using a Bruker DRX 400 NMR spectrometer operating at 400.13 and 100.61 MHz, respectively. Chemical shifts, δ, were quoted in parts per million downfield from TMS and were referenced from the residual solvent peaks ($CHCl_3$: 7.26 ppm; $CHCl_3$: 77.36 ppm; $CDCl_3$: 77.16 ppm) or TMS. Spin multiplicities were indicated by the following symbols: *s* (singlet), *t* (triplet), *m* (multiplet). The melting point was determined in an open glass capillary using an OSI 9100 Electrothermal digital melting point apparatus, and was uncorrected. High resolution mass spectrometry analyses were performed on a Bruker DaltonicsSolariX FT-ICR spectrometer operating at 9.4 Tesla in the Laboratory of Mass Spectrometry of the University of Liège. The Raman spectrum was recorded directly through the glass vial with a Labram 300 (Horiba) Raman spectrometer interfaced with a He-Ne laser (laser line at 632.8 nm) with a power of 4 mW on the sample. The infrared spectrum was obtained with an IS5 instrument (Thermo Scientific) interfaced with an ID7 ATR module equipped with a monolithic diamond ATR crystal.

*2.1. Synthesis, crystallization and characterization of 1,4-Diacetyl-3,6-bis(phenylmethyl)-2,5-piperazinedione (**2**)*

In a one-neck round-bottomed flask equipped with a magnetic bar, was added 3.3 g of L-phenylalanine (2 mmol) and 40 mL of ethylene glycol. The suspension was stirred at 170 °C for 4 h. Afterward, the resulting brown solution was concentrated under high vacuum and cooled at −20 °C overnight. The obtained light brown precipitate was collected by filtration and washed with 50 mL of ethanol and dried under high vacuum. The crude product was allowed to react in the next step without further purification.

To obtain compound **2**, 30 mL of acetic anhydride was added to the collected solid of the previous step and refluxed for 6h. After this period, the solvent is removed by distillation. The crude solid was dissolved in 50 mL of dichloromethane and washed three times with 30 mL of a saturated solution of $NaHCO_3$ and once with 50 mL of water. The organic fraction was dried over $MgSO_4$, filtered and the solvent removed under vacuum to give a viscous orange oil. Silica-gel column chromatography of the oil using as eluent a mixture of petroleum ether and ethyl acetate (8:2.5 v/v) gave **2** as a white crystalline solid (87% overall yield).

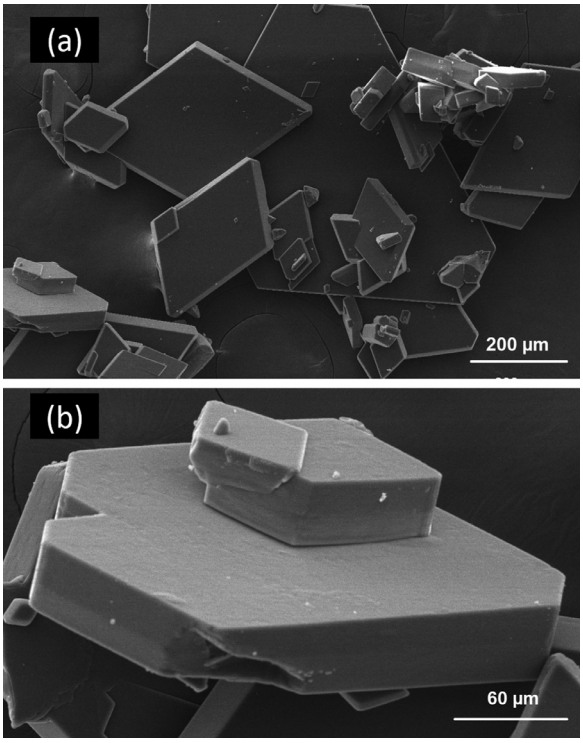

Fig. 2. Scanning electron micrographs of compound **2**.

Analytical data for compound 2: R_F (dichloromethane) 0.7; m.p. 189−192 °C. ^{1}H NMR (400.13 MHz, $CDCl_3$): δ 7.25−7.22 (*m*, 6H, *H*3 + *H*4 + *H*5), 6.91−6.89 (*m*, 4H, *H*2 + *H*6), 4.44 (*t*, *J* = 8 Hz, 2H, *H*8), 3.16−3.14 (*m*, 4H, *H*7), 2.52 (*s*, 6H, *H*11). ^{13}C NMR (101.61 MHz, $CDCl_3$): δ 171.09 (*C*10), 167.78 (*C*9), 134.11 (*C*1), 129.91 (*C*2 + *C*6), 128.85 (*C*3 + *C*5), 128.09 (*C*4), 58.42 (*C*8), 39.99 (*C*7), 27.69 (*C*11) (see Figures S1−S5 in the Supplementary Materials). MS (ESI): m/z calculated for $C_{22}H_{23}N_2O_4^+$ = 379.16578 $[M+H]^+$, found 379.16682 $[M+H]^+$. IR (ν, cm^{-1}): 3396, 3072, 2949, 1703, 1386, 1361, 1223, 1134, 1035, 744, 707, 615 [Fig. 2(b)].

2.2. Scanning electron microscopy

Scanning electron microscopy (SEM) was used to characterize the particle size and morphology of different crystals of **2**. The SEM morphological analyses of the samples were performed in the Laboratoire de Chimie Inorganique Structurale (GreenMAT, CESAM) of the University of Liège, on a FEG-ESEM XL30 (FEI) apparatus with an accelerating voltage of 15 kV under high vacuum. Samples were deposited on carbon tapes. Sputtering deposition was done with gold target under argon atmosphere (Balzers, SCD004, Sputter coater).

2.3. Single-crystal x-ray diffraction analysis

A small portion of **2** was dissolved in dichloromethane and allowed to evaporate slowly at room temperature, yielding crystals suitable for X-ray crystallographic analysis. The data were collected by applying the omega and phi scans method on a Bruker APPEX−II diffractometer using graphite-monochromated Mo-Kα radiation (λ = 0.71073 Å) from a fine-focus sealed tube source at 100 K following the previous report [42]. The structure was solved using SHELXT [43] and finally refined by full-matrix least-squares based on F^2 by SHELXL [44]. An empirical absorption correction was applied using the SADABS program [45]. All non-hydrogen atoms were refined anisotropically and the hydrogen atom positions were included in the model on the basis of Fourier difference electron density maps. All secondary CH_2 and aromatic CH hydrogen atoms were refined using a riding model with $U_{iso}(H)$ = 1.2 $U_{eq}(C)$. The methyl hydrogen atoms were refined as a rigid group with torsional freedom [$U_{iso}(H)$ = 1.5 $U_{eq}(C)$] and the hydrogen H8 atom as a free atom.

Crystal data, data collection and structure refinement details table (Table 1) is constructed using WinGX software [46,47]. The CIF-file for compound **2** containing the supplementary crystallographic data has been deposited into CCDC with number 1870902. These data can be obtained free of charge via http://www.ccdc.cam.ac.uk/conts/retrieving.html (or from the Cambridge Crystallographic Data Centre, 12, Union Road, Cambridge CB2 1EZ, UK; fax: +44 1223 336033).

2.4. Hirshfeld surface analysis

The intermolecular interactions present in the crystal structure of compound **2** were evaluated by drawing contact and shape descriptors using Hirshfeld surface analysis. Molecular Hirshfeld surfaces were calculated using a standard (high) surface resolution and with the three-dimensional d_{norm} surfaces mapped over a fixed colour scale from −0.1369 (red) to 1.1914 Å (blue) with the program CrystalExplorer17 [48].

2.5. Computational details

Geometry optimization of the molecular structure of **2** in the gas phase was performed with the GAUSSIAN 09 revision D.01 at 0 K [49,50]. The DFT method with CAM-B3LYP functional was used and all atoms were described with the 6-311G (D) basis set [51]. The simulated IR spectrum of compound **2** was obtained by applying the fully-automated, second-order vibrational perturbation approach implemented in the GAUSSIAN 09. The uniform scaling factor (0.9456) was used to correct the calculated harmonic frequencies computed at the DFT level.

2.6. Molecular docking studies

Molecular docking calculations were performed with AUTODOCK 4.2 [52] according to the reported method [53]. The cocrystal structure of QZ59 with P-Glycoprotein (PDB code 3G60, resolution of 4.40 Å) retrieved from the protein data bank (PDB) was used in the docking study [54]. All the ligand and water molecules attached to the proteins were removed. The missing hydrogen atoms were added and non-polar hydrogens were merged into their corresponding carbon atoms using AutoDock Tools. A grid box size of 50 × 50 × 50 $Å^3$ was defined around the P-Glycoprotein ligand binding domain. 3D molecular structure of compound **2** obtained from the X-ray crystal structure data was used for the docking.

Robust poses population resulting from 100 runs docking simulation using genetic algorithm were considered for the analyses. The Docking Parameter File (DPF) was generated with Lamarckian genetic algorithm by setting the protein as rigid molecule. Finally, the DLG (Docking Log File) file is created by running Autodock with DPF as input file. Out of several interactions possible, the best pose with lowest binding energy and the most probable was considered for further protein-ligand docking. PyMOL [55] was used for docking conformation representation.

3. Results and discussion

3.1. Synthesis and NMR

The title compound (**2**) was prepared from L-(S)-phenylalanine using the condensation method [17] followed by acetylation

Table 1
Crystal data of 1,4-diacetyl-3,6-bis(phenylmethyl)-2,5-piperazinedione (**2**).

Identification code	NIQHON	
Empirical formula	C22 H22 N2 O4	
Formula weight	378.42	
Temperature	100 K	
Wavelength	0.71073 Å	
Crystal system	Orthorhombic	
Space group	*Pbca*	
Unit cell dimensions	a = 7.8241(3) Å	α = 90 °
	b = 12.3441(5) Å	β = 90 °
	c =19.2615(8) Å	γ = 90 °
Volume	1860.30(13) Å^3	
Z	4	
Density (calculated)	1.351 mg/m^3	
Absorption coefficient	0.094 mm^{-1}	
F(000)	800	
Crystal size	0.52 × 0.43 × 0.16 mm^3	
Theta range for data collection	2.1 to 28.3 °	
Index ranges	-10<=h<=10, -16<=k<=16, -25<=l<=24	
Reflections collected	16262	
Independent reflections	2315 [R(int) = 0.038]	
Completeness to theta = 28.282 °	100 %	
Absorption correction	Semi-empirical, Multi-scan	
Max. and min. transmission	0.888 and 0.959	
Refinement method	Full-matrix least-squares on F2	
Data / restraints / parameters	2315 / 0 / 132	
Goodness-of-fit on F2	1.057	
Final R indices [I>2sigma(I)]	R1 = 0.0388, wR2 = 0.0643	
R indices (all data)	R1 = 0.0472, wR2 = 0.0977	
Extinction coefficient	n/a	
Largest diff. peak and hole	0.29 and -0.21 e.Å^{-3}	

(Fig. 1). In the first step of the synthesis, a suspension of L-phenylalanine in ethylene glycol was heated at 170 °C with stirring for 4 h to give the corresponding cyclodipeptide. The cyclodipeptide intermediate was then acetylated in the presence of acetic anhydride to provide its N,N'-diacetylated derivative. Extraction of the product with dichloromethane followed by purification by column chromatography gave **2** as a white crystalline solid in 87% overall yield.

^{1}H and ^{13}C NMR analyses (see Figures S1−S6 in the Supplementary Materials) of compound **2** provided evidence for the presence of the phenyl rings, as indicated by two multiplets in the range δ 7.25−6.89 ppm in 3:2 proportions, and four signals in ^{13}C NMR between 135 and 128 ppm. As expected, the methyl group of the acetyl substituents resonated as singlets around 2.5 ppm (^{1}H NMR) and 28 ppm (^{13}C NMR). On ^{13}C NMR spectroscopy, the carbonyl groups led to two deshielded singlets at ca. 168 and 171 ppm. The four protons of the two C6H5-CH2- linker are observed as a multiplet around 3.15 ppm. The zoom in of the benzyl protons peaks is provide in Figure S2. Of note, assignment of all the peaks was corroborated by 2D NMR spectroscopy (Figure S5). Finally, the electron-spray ionization mass spectrum showed a peak at m/z 379.16 corresponding to the protonated molecular ion $[M+H]^+$.

3.2. Scanning electron microscopy

The morphology of the crystals obtained after column chromatography was characterized by scanning electron microscopy (SEM). As shown in Fig. 2, the particle sizes are not uniform. The particles exhibit plate-like shape and their thickness is about 40 μm. All the particles possess clean and smooth surface facets, suggesting that they are well crystallized. Moreover, they have similar irregular polyhedral morphologies.

3.3. Crystal structure of 1,4-diacetyl-3,6-bis(phenylmethyl)-2,5-piperazinedione (*2*)

The X-ray diffraction analysis of high quality crystals obtained by slow evaporation of dichloromethane reveals that in 1,4-diacetyl-3,6-bis(phenylmethyl)-2,5-piperazinedione (**2**), the two stereocentres are of opposite configuration, R and S, whereas initially only L-(S)-phenylalanine was used for the synthesis. Obtaining the meso compound was confirmed by its zero optical rotation. Inversion of stereochemistry at the chiral carbon in the α-position of a carbonyl group is quite common and has been described several times in the synthesis of DKPs [16]. The X-ray diffraction analysis also reveals that product **2** crystallizes in the centrosymmetric orthorhombic space group (Pbca), with half of the molecule in the asymmetric unit around an inversion centre located at the centroid of the diketopiperazine ring. A perspective view and atom labelling of the X-ray crystal structure of **2** is shown in Fig. 3a. Selected interatomic bond distances and angles are given in Table 2.

Table 2
Selected bond lengths (Å) and bond angles (°) in compound **2**.

Bond lengths (Å)		Bond angles (°)	
C1-C7	1.5064 (16)	C1−C7−C8	113.01 (9)
C7−C8	1.5547 (16)	N1^i−C8−C9	116.51 (9)
C8−N1^i	1.4690 (14)	N1^i−C8−C7	110.38 (9)
C8−C9	1.5160 (16)	C9−C8−C7	107.34 (9)
C9−O1	1.2122 (13)	O1−C9−N1	123.95 (10)
C9−N1	1.3855 (14)	O1−C9−C8	117.87 (10)
N1−C10	1.4235 (15)	N1−C9−C8	117.86 (9)
C10−O2	1.2104 (14)	C9−N1−C10	124.49 (9)
C10−C11	1.4957 (16)	C9−N1−C8^i	120.98 (9)
		C10−N1−C8^i	114.52 (9)
		O2−C10−N1	118.21 (10)

In round brackets are the estimated standard deviations. Symmetry code: *–x, –y, –z*.

From the data collected in Table 2, it is apparent that all the C−N bond distances are different, especially those of the C9−N1 [1.3855 (14) Å] and N1−C10 [1.4235 (15) Å] bonds of the imide group. Comparative study with similar derivatives highlight a distinctive characteristic of the 1,4-diacetyl-2,5-piperazinedione core. As in the analogues **3** - **6** (Fig. 4) [33,34] the endocyclic C(O)−N bond is shorter compared to the exocyclic one. The increased double-bond character in the endocyclic C(O)−N bond presumably

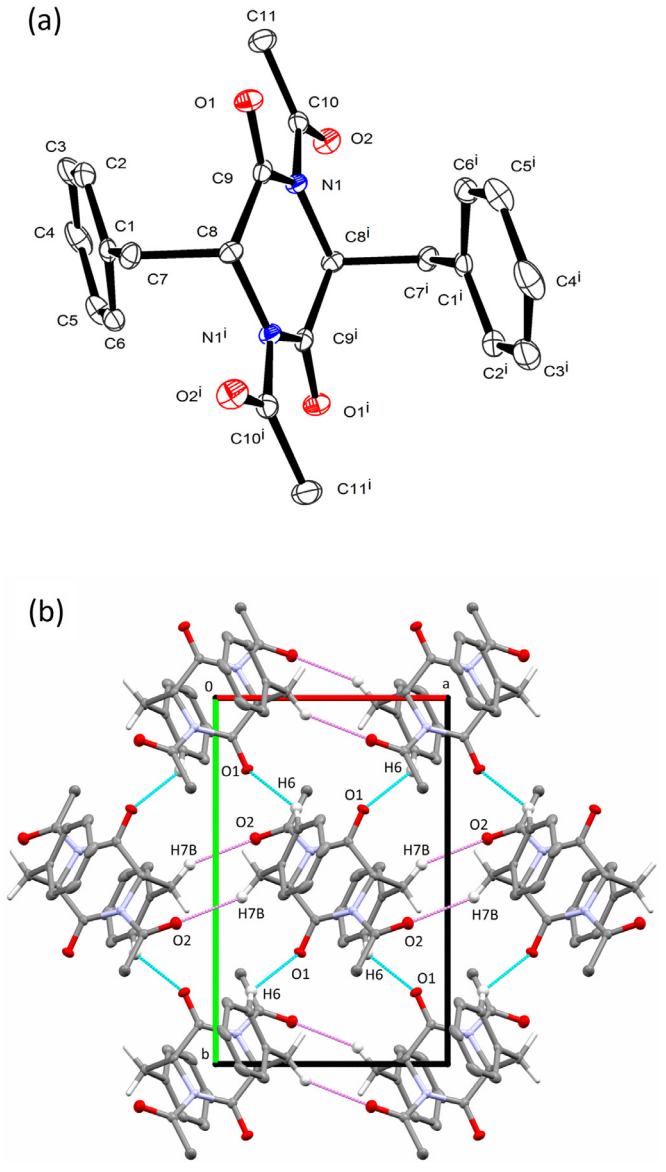

Fig. 3. (a) The molecular structure of compound **2**, showing the atom-labelling scheme. Displacement ellipsoids are drawn at the 50% probability level. Symmetry code: *–x, -y, -z*. (b) Intermolecular C7−H7B···O2 (violet) and C6−H6···O1 (cyan) H-bond interactions along the *ab* plane of the crystal packing of compound **2**.

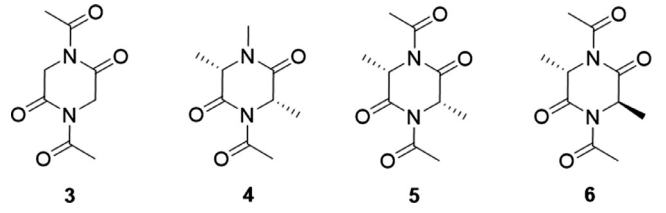

Fig. 4. Structures of some reported 1-acetyl- and 1,4-diacetyl-2,5-piperazinedione analogues.

reflects the enhanced delocalization of the lone pair of electrons of the nitrogen atom onto the endocyclic imide linkage. The third C−N bond, C8−N1^{i}, is the longest with a length of 1.4690 (14) Å in the range of those observed for related compounds [56,57].

From the value of the torsion angle C8−C9−N1−C8^{i} which measures the deviation of the amide bond from planarity, it is apparent that the endocyclic amide linkage C9−N1 is twisted as characterized by the large ω value [−25.01 (16) °]. The dihedral angles C9^{i}−N1^{i}−C8−C9 and N1^{i}−C8−C9−N1 are also close to 25 ° [−24.69 (15) ° and 23.90 (15) °, respectively], but opposite in sign, thus leading to a succession of internal rotation angles around the ring with alternating positive and negative signs, suggesting a flattened chair conformation of the diketopiperazine ring. Further examination of the parameters given in Table 2 shows that the internal bond angle N1^{i}−C8−C9 is 116.51 (9) °, a value close to that measured for related compounds, and that the internal bond angle C9−N1−C8^{i} is slightly compressed in **2** as in analogues **5** and **6** (Fig. 4), i.e. 120.98 (9) ° vs 119.8 and 120.3 ° [58]. On the other hand, a very low deviation of the acetyl group from the plane C9−N1−C8^{i} was observed as evidenced by the torsion angle C9−N1−C10−C11 of −2.05 (16) °.

Table 3
H-Bond interactions in compound **2**.

D*−H···*A	C6−H6···O1	C7−H7B···O2
[Symm]	[−1/2 − *x*, 1/2 + *y*, *z*]	[−1 + *x*, *y*, *z*]
***D*−H (Å)**	0.95	0.99
H···*A* (Å)	2.52	2.55
***D*···*A* (Å)**	3.3368 (14)	3.4413 (14)
***D*−H···*A* (°)**	144	150

The crystal packing of **2** is stabilized by short intermolecular interactions along the ab plane (Fig. 3b). Thus, H-bond interactions (C7−H7B···O2, Table 3) are present along the a axis, between a benzyl H atom of one molecule and the oxygen atom of the acetyl group of an adjacent molecule. In addition, there is another intermolecular H-bond interaction between each carbonyl oxygen of the DKP ring of one molecule and the hydrogen at C6 of the phenyl group of another molecule (C6−H6···O1). These interactions lead to a succession with right, then inverted disposition of the molecules in the cell providing thereby high stabilisation to the crystal packing.

Furthermore, examination of X−H···Cg(π-ring) distances reveals the existence of an additional interaction between C4−H4 and the π electrons of the aromatic ring (C1→C6) [51] of a neighboring molecule (0.5 + x, y, 0.5 − z). This contact is characterized by short distances (dπ_cH) of 2.88 Å between H4 and the centroid of the phenyl ring with an angle of 136 ° between the C4−H4 bond and the ring center (Figure S7). The perpendicular distance (H_{perp}) between H4 and the plane of the phenyl ring is 2.79 Å and the angle of approach of the vector Hπ_c to the plane of the aromatic ring (θ) is 75.97 °, indicating that hydrogen H4 is located above the center of the ring and that the C4−H4 bond points towards a ring carbon. Altogether, this interaction as well as the dihedral angle C1−C7−C8−C9 (54.54 °) could explain why the molecule adopts a folded *S* shape with the two phenyl rings folded over and under the diketopiperazine ring.

3.4. Conformational and DKP ring puckering analysis

The particular folded conformation adopted by compound **2** let us to investigate the DKP ring puckering. The calculated Cremer and Pople puckering parameters [59,60] indicate that the DKP ring of compound **2** adopts a flattened chair conformation with Θ = 0.00 ° and a total puckering amplitude (Q) = 0.2233 (11) Å. Very close values were found for *trans*-(*R,S*)-1,4-diacetyl-3,6-dimethylpiperazine-2,5-dione (**6**) (Fig. 4), in which positions 3 and 6 of the DKP ring are substituted by methyl groups in the *trans* configuration, implying therefore that intermolecular interactions do not play a significant role in the conformation of the DKP ring. This is in contrast to the boat conformations adopted by 1,4-diacetylpiperazine-2,5-dione (**3**) [61] and *cis*-(*S,S*)-1,4-diacetyl-3,6-dimethylpiperazine-2,5-dione (**5**) (Fig. 4). Importantly, in these compounds, carbons 3 and 6 are not substituted (compound **3**) or

Table 4
Calculated and experimental torsion angles (°) in compound **2**.

Angle	Definition	Optimized structure	X-ray structure
ω_1	C8–C9–N1–C8^i	−21.72	−25.01 (16)
ω_2	C8^i–C9^i–N1^i–C8	21.72	25.01 (16)
ψ_1	N1–C8^i–C9^i–N1^i	−20.57	−23.89 (15)
ψ_2	N1^i–C8–C9–N1	20.57	23.90 (15)
ϕ_1	C9–N1–C8^i–C9^i	21.24	24.69 (15)
ϕ_2	C9^i–N1^i–C8–C9	−21.24	−24.69 (15)
α_1	C8–C9–N1–C10	158.71	156.06 (10)
α_2	C8^i–C9^i–N1^i–C10^i	−158.71	−156.06 (10)
β_1	C1–C7–C8–C9	60.26	54.54 (12)
β_2	C1^i–C7^i–C8^i–C9^i	−60.26	−54.54 (12)
γ_1	O1–C9–N1–C10	−15.67	−17.21 (17)
γ_2	O1^i–C9^i–N1^i–C10^i	15.67	17.21 (17)

Symmetry code: *–x*, *–y*, *–z*.

possess a methyl group in the *cis* position (compound **5**), demonstrating thereby the crucial role played by N and/or α-C substituents in determining the conformations of diketopiperazines.

The preference for an aromatic part of an amino acid residue like phenylalanine and tyrosine to fold over the DKP skeleton is previously reported [62]. The folded conformation has been observed both in the solid state and in solution. This phenomenon is not well understood and plausible explanations have been proposed. First, NMR studies reported by Kopple and Marr [63] indicated that this folded form was favored over other possible conformations of the arylmethyl side chain by an enthalpy change resulting from a direct rather than solvent-mediated interaction between the aryl and DKP rings [64]. Because of the aromatic nature of phenylalanine, attractive forces between the two rings [64] as well as dispersion forces favoring, among others, CH···π non-covalent interactions [39] have also been recognized as important factors in the stabilization of the folded conformation. In the case of compound **2**, the CH···π interaction could not be suggested (C8–H8···π; dπ_cH = 3.805 Å; d = 1.275 Å; α = 96.65 °, θ = 70.42 °). Budesinsky also suggested that, to escape repulsion with the vicinal carbonyl group, the benzyl side-chain of the phenylalanine residue prefers the pseudo-axial orientation and is stacked over the DKP ring, consistent with a presumed face-to-face attractive interaction between the phenyl and DKP rings [37]. For compound **2**, the calculated geometric parameters (Cg–Cg = 3.625 Å, α = 44 °, β = 8.8 °, γ = 45 °, CgI_Perp = 2.562 Å, CgJ_Perp = −3.562 Å) are compatible with an intramolecular interaction between the phenyl and DKP rings and this could finally explain why *complete* inversion of stereochemistry at one chiral C$_\alpha$ carbon center occurred during its synthesis from optically pure L-(*S*)-phenylalanine.

3.5. DFT molecular modeling

The structure of the DKP **2** was optimized at the 6-311G (D) level using CAM-B3LYP functional of the DFT method in the gas phase. The optimized structure of **2** was obtained showing "*trans*-phenyl conformations" (Fig. 5a). Superimposition of the crystallographic (in black) with optimized (in grey) structures of compound **2** presented in Fig. 5b show good agreement. The slight differences with the experimental X-ray structure comes from the effects of crystal packing. Actually, the conformations assumed by the diketopiperazine ring are best described by the values of the torsion angles ω, ψ, and ϕ (Fig. 5e), and these are summarized in Table 4.

For the optimized structure, all ω_i, ψ_i, and ϕ_i values (i = 1 or 2) are generally close to those obtained from the X-ray data of compound **2** (Table 4). These similarities reveal that the optimized structure is symmetrical as the crystal structure of **2**. Fig. 8b shows the satisfactory match between the theoretical and the crystal structure of **2**, which indicates that intermolecular interactions

Table 5
Global reactivity descriptor of compound **2**.

Parameters (eV)	Values
E_{LUMO}	-1.885
E_{HOMO}	-9.012
Energy band gap $\lvert E_{HOMO}\text{-}E_{LUMO}\rvert$	7.127
Ionization potential ($I = -E_{HOMO}$)	9.012
Electron affinity ($A = -E_{LUMO}$)	1.885
Chemical hardness (η = (I-A)/2)	3.563
Chemical softness ($z = 1/2\eta$)	0.140
Electronegativity ($c = (I + A)/2$)	8.069
Chemical potential ($\mu = -(I + A)/2$)	-8.069
Electrophilicity index $\omega = \mu^2/2\eta$	9.128
Maximum charge transfer index ($\Delta N_{max} = -\mu / \eta$)	2.265

are not at the origin of the *S* form adopted by the molecule, as suggested above. Furthermore, one can suggest an interactions between the acetyl oxygen O2 and hydrogen H8 located in the α position of the amide group. Indeed, atoms O1, H8, and O2 are practically aligned (angle O1···H8···O2 = 170.8 °). With an angles C8–H8···O1 of 70.27 ° and C8–H8···O2 of 100.57 °, this disposition is probably due to internal geometrical constraints. These intramoleculars orientation in compound **2** have also the effect of moving the methyl group away from the DKP ring and thus avoiding steric repulsion between the methyl and phenyl substituents.

3.6. Frontier molecular orbital

The frontier molecular orbitals formed by the Highest Occupied Molecular Orbital (HOMO) and the Lowest Unoccupied Molecular Orbital (LUMO) are the most important molecular orbitals contributing in the chemical reactivity. The energy of the HOMO level is linked to the ionization potential, whereas the LUMO energy level is linked to the electron affinity. The gap between HOMO and LUMO energies level of a selected compound characterizes therefore the molecular chemical stability [65]. A large gap suggests good stability and lower reactivity of the compound in chemical reactions. Other parameters of reactivity relative to these orbitals and the relation are reported in Table 5. The HOMO and LUMO molecular orbitals of **2** have been calculated and presented in Fig. 5c and 5d. The LUMO orbitals are mainly localized over the DKP ring and acetyl units. The results gave and HOMO and LUMO orbitals energies levels values of -9.012 eV and -1.885 eV respectively giving an energy gap of 7.127 eV. This gap value reveals a good stability of **2**.

3.7. IR and Raman spectroscopy

The new compound is also characterized by IR and Raman spectroscopy. In the IR and Raman spectra of compound **2** (Fig. 6), the most intense absorption located around 1710 cm^{-1} was assigned to the stretching of the carbonyl groups [66–68]. Note that only one strong absorption (1714 cm^{-1} in Raman and 1703 cm^{-1} in IR) is obtained for both endocyclic and exocyclic carbonyl groups in **2** (Figs. 6a and 6b), while two strong bands resulting from asymmetric and symmetric stretch were normally expected as in imides [56,69,70] and anhydrides [71]. In addition, the in-plane deformation vibrations of C=O that is expected in the region 625 ± 70 cm^{-1} is obtained at 707 cm^{-1} in IR (692 cm^{-1} in Raman). The only one peack obtained in Raman and infrared spectroscopy for carbonyl group can be attributed to the symmetry present in the molecule in addition to the C=O bond lengths (C9–O1 and C10–O2) that are practically identical [1.2122 (13) and 1.2104 (14) Å, respectively]. The strecking corresponding to N–C bond is observed at 1386 cm^{-1} in IR and 1372 cm^{-1} in Raman. The aromatic C=C-C and C=C stretching vibrations of phenyl in **2** correpond to

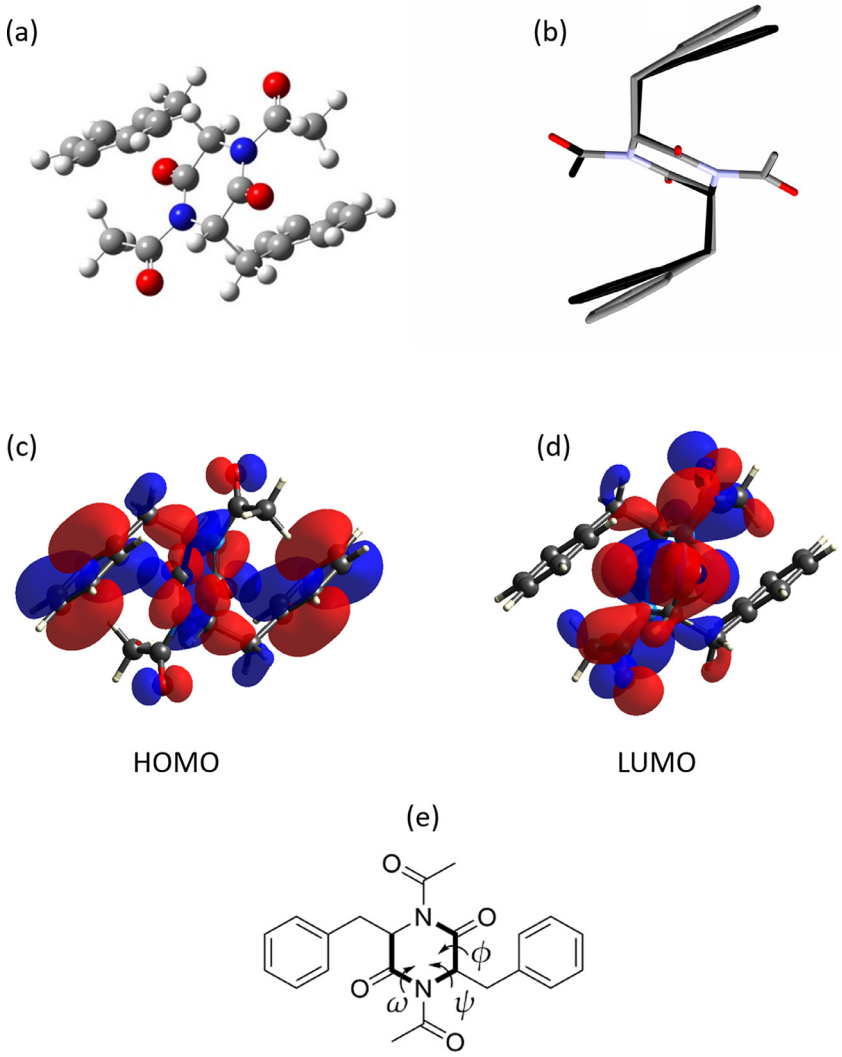

Fig. 5. Calculated optimized structures (a), overlay of the crystallographic (in black) with optimized (in grey) structures of compound **2**. Frontiers HOMO (c) and LUMO (d) molecular orbital of **2** and torsion angle definition (e).

the peacks at 1223 and 1134 cm^{-1} respectively in IR spectrum. These vibrations are observed at 1212 and 1116 cm^{-1} respectively in Raman. Much less informative absorptions included weak C–H stretching vibration bands between 2800 and 3100 cm^{-1} for the various alkyl and phenyl substituents. The very low intensity band observed around 3396 cm^{-1} in IR spectra could be attributed to water O-H vibration coming from the adsorption of water by compound **2** [72,73]. The simulated IR spectrum present in Figure 10c shows very good agreement with the experimental. By the way, a single peak in the ν(CO) stretch region at 1700 cm^{-1} was also displayed in the simulated IR spectrum of **2** (Fig. 6c). The similarity between the experimental and theoretical IR spectra reflect also a good agreement of the obtained theoretical structure.

3.8. Hirshfeld surface analysis

The nature and amount of intermolecular interactions in the crystal packing of compound **2** were described using Hirshfeld surface (HS) analysis. The d_{nom} (normalized contact distance) is obtained by considering the global relation between the distances of any surface point to the nearest interior (d_i) and exterior (d_e) atom and the Van der Waals radii of the atoms. In addition, HS mapped with shape index and curvedness (Fig. 7) were used to complete the non-covalent interactions in the molecular packing [74–76].

The HS mapped over d_i shows multiple red spots distributed on the surface (Fig. 7), revealing that most of the atoms of **2** are closed to the surface. The same tendency is observed on the surface mapped over d_e (Fig. 7) demonstrating that neighbor's nuclei are also close to the surface. The intermolecular interactions were then analyzed through the mapping of d_{norm} by considering the contact distances d_i and d_e from a point on the surface to the nearest nucleus inside and outside the surface, respectively. The surface mapped over d_{norm} highlights well-defined red spots corresponding to intermolecular distances shorter than the sum of the van der Waals radii (Fig. 7). These dominant interactions are intermolecular C—H···O and O···H—C hydrogen bonds. The white spots and blue regions on the surface reveal distances equal to and longer than the sum of the van der Waals radii, respectively [74,77].

According to the Hirshfeld surface of compound **2** mapped with the shape index (−1.0 to 1.0 Å) (Fig. 7), convex blue regions correspond to hydrogen-donor groups, whereas concave red regions correspond to hydrogen-acceptor groups. In addition, the decomposition of the Hirshfeld surface mapped over shape index confirms the existence of C4—H4···π interactions as discussed in the X-ray structural description section (Fig. 7). The curvedness that measures "how much shape" property was obtained on the HS and shown in Fig. 7. The absence of large flat areas on the surface (low values of curvedness) reveals a lack of π–π planar stacking

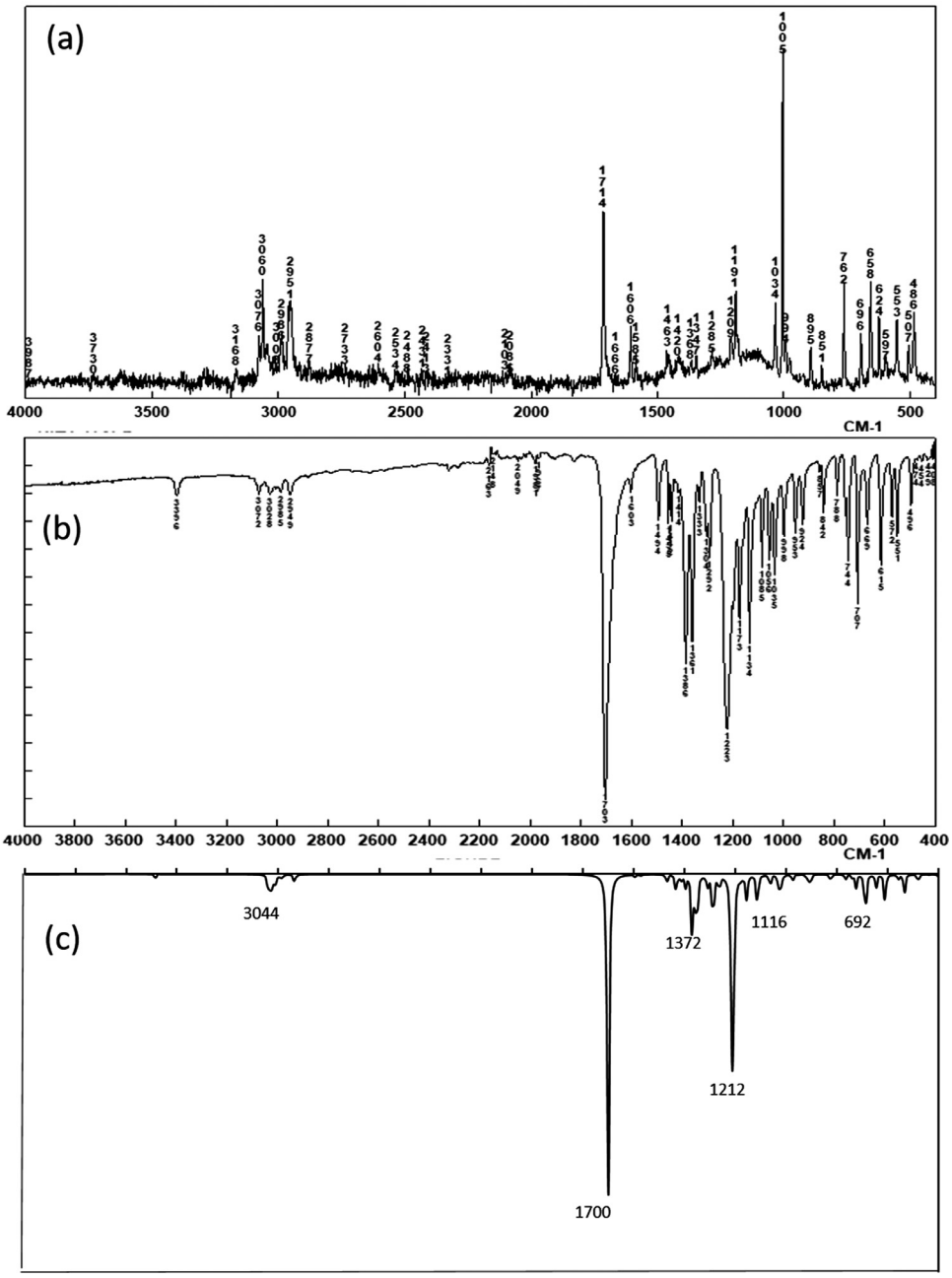

Fig. 6. Experimental Raman (a) and infrared (b) spectra of compound **2**, together with its simulated infrared spectrum (c).

contact. In contrary, many curvatures domains divide the surface into patches that could associated with low interaction with other molecules.

The distances from the HS to the nearest nucleus inside the surface (d_i) and outside the surface (d_e) are used in CrystalExplorer program to generate a 2D histogram named molecular fingerprint [77,78]. Since there is the immediate environment providing the various contacts of the selected molecule is used to construct the fingerprint, this latter is unique and allows to evaluate the contributions of interatomic contacts to the HS. The full and decomposed fingerprint plots with the percentage values calculated for all intermolecular contacts are shown in Fig. 7. The results reveal that the major contributions to the Hirshfeld surface are from H···H contacts (58.2%), H···O/O···H (24.8%) and C···H/H···C interactions (14.2%). The other intermolecular contacts contribute little to the overall fingerprint plot and appear insignificant.

3.9. Electrostatic potential and crystal voids

In addition to molecular orbital, molecular properties could be described by mapping the molecular electrostatic potential that play a key role for identify reactive positions on the molecular surface [79]. This map is useful to predict the position of nucleophile and electrophile attack. The molecular electrostatic potential of compound **2** is calculated at B3LYP/6–31G(d,p) level of theory and mapped on the Hirshfeld surfaces (Fig. 7). The blue and red regions around the different atoms observed on the surface correspond to positive and negative electrostatic potentials respectively. It appears clearly that, the electron-rich site are mainly localized around the oxygen atoms.

The folding observed in the conformation adopted by the described DKP, the intermolecular contact and the position of electron rich sites provide particular stacking in the crystal that could

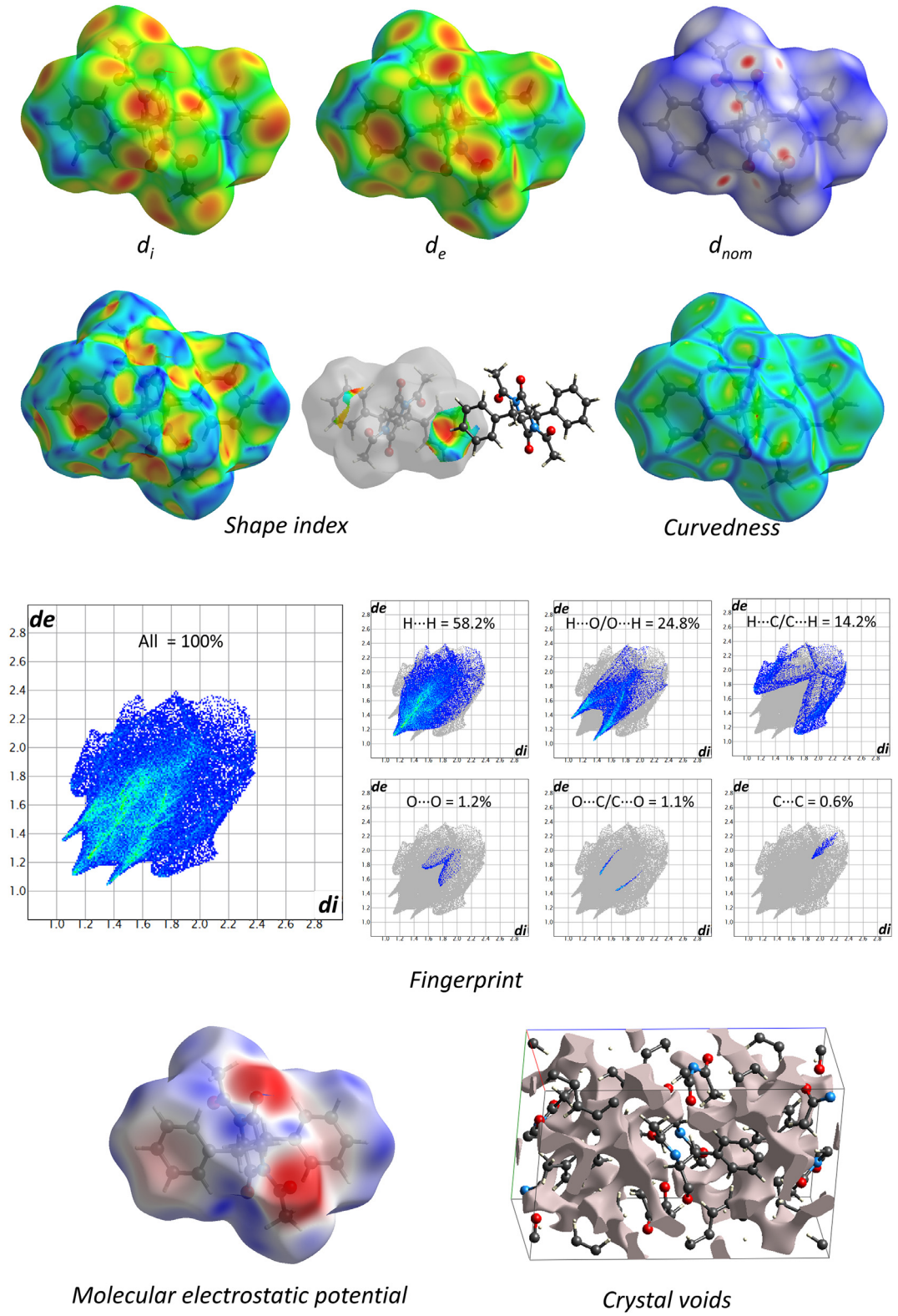

Fig. 7. Three-dimensional Hirshfeld surface of compound **2** mapped over d_i (in the range 1.0532 to 2.4216 A, d_e (in the range 1.0546 to 2.191 A), d_{norm} (in the range -0.1370 to 1.1914), shape-index (-1.000 to 1.000), shape index highlighting C4-H4···Cg contacts as red spots (Symmetry: 0.5 + x, y, 0.5 – z) and curvedness (in the range of -4 to 4). The two-dimensional fingerprint plots of compound **2** and the decomposed contributions. Molecular electrostatic potential (-0.0567 to 0.0450 a.u.) and crystal voids present in the title compound **2.** The surfaces are transparent to allow visualization of the molecule.

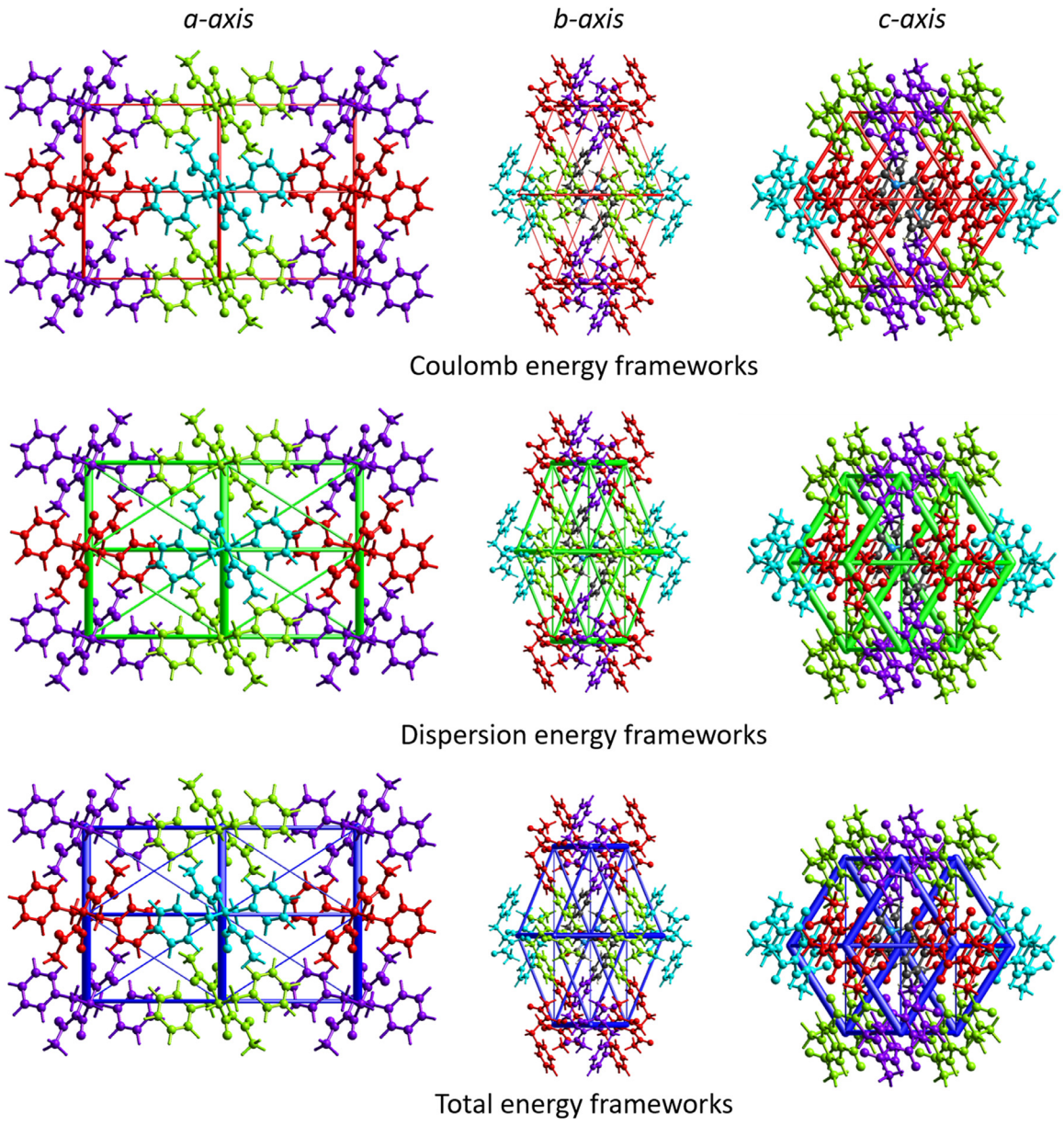

Fig. 8. The color-coded interaction energy frameworks of compound **2** viewed along the crystallographic a, b and c axes. Energy framework diagram for electrostatic, dispersion and total interaction energy. The energy factor scale is 80 and the cut-off is 5.00 kJ/mol.

describe by analyzing the voids in the crystal structure. A view of crystal voids present in **2** is shown in Fig. 7. The voids parameters of the title compound gave void volume of 193.70 A^3, an area of 649.81 A^2, a globularity of 0.249 and asphericity value of 0.183. Thank to these values, low voids percentage of 10% was obtained attesting the effect of molecular folding and a compact stacking of the molecules in the crystal structure.

3.10. Interaction energy framework

The various intermolecular contacts depicted in the structural and packing stabilization of this novel DKP are governed by interaction energies that could be computed and present graphically as energy diagrams. Therefore, the intermolecular interactions energies of **2** were calculated using CE-B3LYP/6–31G(d,p) energy model available in CrystalExplorer [80]. The 3D topology of the energy framework of compound **2** is presented on Fig. 8. The radii of the cylinders are proportional to the magnitude of interaction energy. The selected compound (in black) is surrounded by molecules color coded according to their interaction energy within a cluster of radius of 3.8 Å. As defined by Spackman and Mackinzie, the total intermolecular energy E_{tot} (kJ/mol) relative to the reference molecule (in black) is obtained by summing the energies of four main components, comprising electrostatic (E_{ele}), polarization (E_{pol}), dispersion (E_{dis}) and exchange-repulsion (E_{rep}) with scale factors of 1.057, 0.740, 0.871 and 0.618, respectively [81,82]. The different energy components are resumed in Table S1.

The graphical representation of Coulomb interaction energy (red), dispersion energy (green) and total interaction energy (blue) of **2** viewed down *a, b* and *c* axes are presented in Fig. 8. The values of the total energy components are -34.4 kJ/mol, -9.0 kJ/mol, -104.9 kJ/mol, 71.6 kJ/mol for E_{ele}, E_{pol}, E_{dis} and E_{rep} respectively. Altogether, the total interaction energy of -90.1 kJ/mol is obtained. Thanks to the symmetry present in the crystal packing only four different interactions color coded molecules are observed. The interaction with molecules colored in green is the much stronger (-40.1 kJ/mol) and is characterized by the lowest distance between molecular centroids (7.31 Å) with the mu-

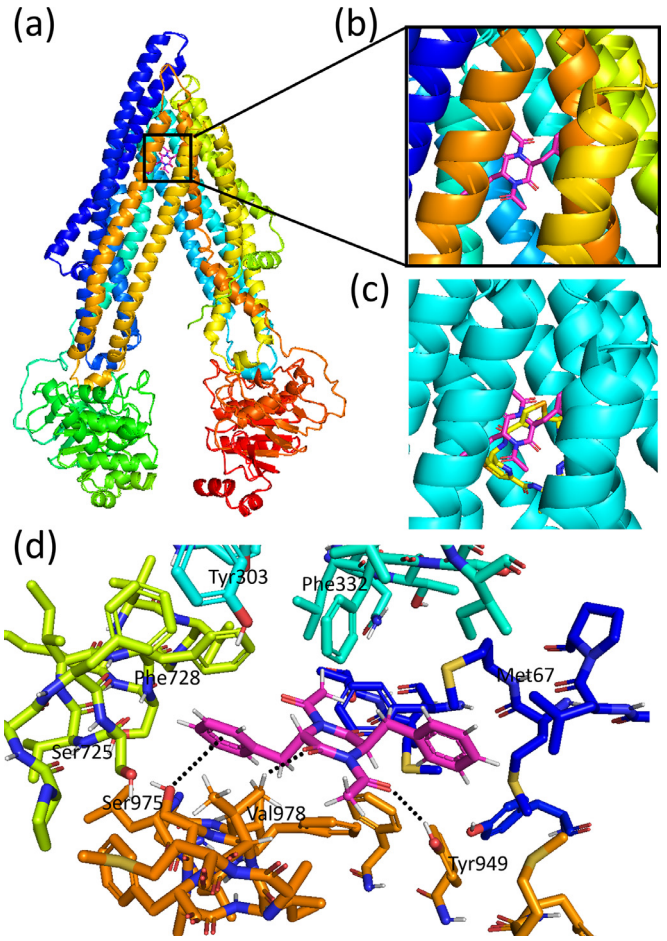

Fig. 9. (a) Cartoon representation of the docked DKP **2** (in magenta) with BCRP. (b) Zoom on the modulator binding site containing compound **2**. (c) Superimposition of the domain occupancy of **2** (in magenta) and TPSA (in yellow). (d) View showing amino acids that could interact with the docked molecule and the probable interactions highlighted as dash black dots lines.

tual C7−H7B···O2/O2···H7B−C7 intermolecular HBs as described above. Although the topology of the coulomb and dispersion energy frameworks seems to be similar, an additional interaction are present in the second one forming a diagonal line within the principal rectangular grid. As a main contributor in the total interaction energy, the same topology of the dispersion energy is observed for the total energy.

3.11. Molecular docking study

Numerous DKP derivatives are described to exhibit anticancer activity. In this work, we explore the possible binding mode of the DKP **2** as novel inhibitor of breast cancer resistance protein (BCRP). The molecular docking results showed that compound **2** can easily enter the BCRP active site (Fig. 9a and 9b). The docking solution of **2** in the active site is therefore compared to the position of TPSA a well know DKP inhibitor of BCRP. As shown in Fig. 9c, the acetylated DKP **2** occupy the same binding domain like TPSA. In the active site, the compound **2** is surrounded by various close residues (Met67, Tyr303, Phe332, Ser725, Phe725, Phe728, Tyr949, Ser975, Val978). One oxygen atom of the acetyl group of **2** could form a hydrogen bond with the residue Tyr949. Furthermore, the contact between one endocyclic oxygen of the DKP ring with Val978 is suggested (Fig. 9d). This contact and the proximity of Phe728 are interesting since Aller and coworkers showed that these residues play an important role in drugs binding mechanism of BCRP [54]. In addition, one oxygen of Ser975 is pointed toward the center of one phenyl ring of **2** leading to a probable $\pi\cdots\pi$ interaction. A relative suitable binding energy (-8.96 kcal/mol), ligand efficiency (-0.32) and inhibition constant (0.272 μM) were obtained for the best pose used for the analysis. The binding domain occupied by **2** in BCRP and the relative energy are consistent with the studies of Fani et al. for another DKP derivatives [26]. The docking results suggest clearly that compound **2** can interact with BCRP active site and could therefore could be consider as inhibitor candidate of this protein.

4. Conclusion

In this study, a novel *N,N'*-diacetylated cyclodipeptide 1,4-diacetyl-3,6-bis(phenylmethyl)-2,5-piperazinedione **2** has been prepared exclusively as the (*R,S*)-stereoisomer starting from the optically pure L-(*S*)-phenylalanine. X-ray diffraction analysis confirm the optical rotation result establishing complete inversion of stereochemistry at the chiral carbon center of one phenylalanine residue. The intermolecular H-bond interactions with oxygen atoms as well as intermolecular C−H···π interactions with the phenyl rings stabilizing the crystal packing are discussed. In addition, suggested intramolecular $\pi\cdots\pi$ interaction information is provided and its analysis combined to describe the compact "*S*" shaped conformation observed in **2** with the two phenyl residues folded facing the diketopiperazine ring. Results demontrated that the title compound possesses a symmetry center located at the centroid of the DKP ring. Analyses of DKP ring puckering using the Cremer and Pople puckering parameters gave values of $\Theta = 0.00\,^{\circ}$ and $Q = 0.2233\ (11)$ Å highlighting a flattened chair conformation. DFT calculations of the structural features and infrared spectroscopy results show very good agreement with the X-ray structure and experimental measurements. The energy gap of the HOMO and LUMO orbitals (7.127 eV) reveals a good stability of the described DKP. To get more insight on compound **2**, the various intermolecular interactions in the crystal packing were further analyzed by mapping contact descriptors (d_{nom}, d_i, d_e) and shape property (shape-index, curvedness) on the Hirshfeld surface and the 2D fingerprint. The analysis of the fingerprint revealed that interactions are dominated by H···H, H···O/O···H and C···H/H···C contacts. In addition, the calculated ESP surface of **2** showed that electron rich domains are mainly located around the oxygen atoms. The first topology of interaction energies stabilizing the structural and packing were obtained and presented graphically as energy framework diagrams. Finally, as potential anticancer molecule, this study provide the molecular docking of **2** with BCRP. The results showed that **2** could bind with the BCRP active site especially with residues Phe728, Tyr949, Ser975 and Val978 and could be consider as inhibitor candidate of this protein.

Other symmetric with or not acetylated DKP are currently in preparation in view to elucidate their structure. In addition, the binding mode of **2** with BCRP reported here will be confirmed by pharmacological in *vitro* testing. Since *cyclo* Phe-Phe is described to exhibit antidepressant and antidementia activity and thanks to the wide range of biological activity exhibited by DKP derivatives, in *vitro* and in *vivo* studies will be conducted to depict the ability of **2** to cross blood brain barrier and especially as neuroprotective agent, but also to study its interaction with AMPA receptors.

Author Contributions

Koffi Sénam Etsè: Investigation; Conceptualization; Data curation; Formal analysis; Writing – original draft; Writing – review & editing;

Guillermo Zaragoza: Crystal data collection and analyses.

Declaration of Competing Interest

The authors declare that there are no conflicts of interest regarding the publication of this article.

Acknowledgments

The authors thank the University of Liège for supporting this research work by letting us to access to most of the platform facilities, C. Malherbe (Laboratoire de Chimie Analytique Inorganique, MolSys, University of Liège) for IR and Raman analyses, and C. Karegeya (Laboratoire de Chimie Inorganique Structurale, GreenMAT, CESAM, University of Liège) for SEM micrographs.

Supplementary materials

Supplementary material associated with this article can be found, in the online version, at doi:10.1016/j.molstruc.2021.131435.

References

[1] M.B. Martins, I. Carvalho, Diketopiperazines: Biological activity and synthesis, Tetrahedron 63 (2007) 9923–9932.
[2] C. Cornacchia, I. Cacciatore, L. Baldassarre, A. Mollica, F. Feliciani, F. Pinnen, 2,5-Diketopiperazines as neuroprotective agents, Mini-Rev. Med. Chem. 12 (2012) 2–12.
[3] W.-R. Abraham, Controlling pathogenic Gram-negative bacteria by interfering with their biofilm formation, Drug Des. Rev. 2 (2005) 13–33.
[4] M.P. de Carvalho, W.-R. Abraham, Antimicrobial and biofilm inhibiting diketopiperazines, Curr. Med. Chem. 19 (2012) 3564–3577.
[5] S.N. Kumar, B. Nambisan, Antifungal activity of diketopiperazines and stilbenes against plant pathogenic fungi in vitro, Appl. Biochem. Biotechnol. 172 (2014) 741–754.
[6] I.A.M. Asiri, J.M. Badr, D.T.A. Youssef, Penicillivinacine, antimigratory diketopiperazine alkaloid from the marine-derived fungus Penicillium vinaceum, Phytochem. Lett. 13 (2015) 53–58.
[7] E. van der Merwe, D. Huang, D. Peterson, G. Kilian, P.J. Milne, M. Van de Venter, C. Frost, The synthesis and anticancer activity of selected diketopiperazines, Peptides 29 (2008) 1305–1311.
[8] S.N. Kumar, C. Dileep, C. Mohandas, B. Nambisan, J. Ca, Cyclo(D-Tyr-D-Phe): A new antibacterial, anticancer, and antioxidant cyclic dipeptide from Bacillus sp. N strain associated with a rhabditid entomopathogenic nematode, J. Pept. Sci. 20 (2014) 173–185.
[9] L. De Petrocellis, F.J. Arroyo, P. Orlando, A. Schiano Moriello, R.M. Vitale, P. Amodeo, A. Sánchez, C. Roncero, G. Bianchini, M.A. Martin, P. López-Alvarado, J.C. Menéndez, Tetrahydroisoquinoline-derived urea and 2,5-diketopiperazine derivatives as selective antagonists of the transient receptor potential melastatin 8 (TRPM8) channel receptor and antiprostate cancer agents, J. Med. Chem. 59 (2016) 5661–5683.
[10] K.C. Nicolaou, M. Lu, S. Totokotsopoulos, P. Heretsch, D. Giguère, Y.-P. Sun, D. Sarlah, T.H. Nguyen, I.C. Wolf, D.F. Smee, C.W. Day, S. Bopp, E.A. Winzeler, Synthesis and biological evaluation of epidithio-, epitetrathio-, and bis-(methylthio)diketopiperazines: Synthetic methodology, enantioselective total synthesis of epicoccin G, 8,8'-epi-ent-rostratin B, gliotoxin, gliotoxin G, emethallicin E, and haematocin and discovery of new antiviral and antimalarial agents, J. Am. Chem. Soc. 134 (2012) 17320–17332.
[11] X. Chen, L. Si, D. Liu, P. Proksch, L. Zhang, D. Zhou, W. Lin, Neoechinulin B and its analogues as potential entry inhibitors of influenza viruses, targeting viral hemagglutinin, Eur. J. Med. Chem. 93 (2015) 182–195.
[12] A. Minelli, I. Bellezza, S. Grottelli, F. Galli, Focus on cyclo(His-Pro): History and perspectives as antioxidant peptide, Amino Acids 35 (2008) 283–289.
[13] S. Manchineella, C. Voshavar, T. Govindaraju, Radical-scavenging antioxidant cyclic dipeptides and silk fibroin biomaterials, Eur. J. Org. Chem. 2017 (2017) 4363–4369.
[14] C. Prasad, Bioactive cyclic dipeptides, Peptides 16 (1995) 151–164.
[15] C.J. Dinsmore, D.C. Beshore, Recent advances in the synthesis of diketopiperazines, Tetrahedron 58 (2002) 3297–3312.
[16] P.M. Fischer, Diketopiperazines in peptide and combinatorial chemistry, J. Peptide Sci. 9 (2003) 9–35.
[17] A.D. Borthwick, 2,5-Diketopiperazines: Synthesis, reactions, medicinal chemistry, and bioactive natural products, Chem. Rev. 112 (2012) 3641–3716.
[18] J.H. Birkinshaw, Y.S. Mohammed, Studies in the biochemistry of micro-organisms. 111. The production of L-phenylalanine anhydride (cis-L-3,6-dibenzyl-2,5-dioxopiperazine) by Penicillium nigricans (Bainier) thom, Biochem. J. 85 (1962) 523–527.
[19] F. Zhu, Y.C. Lin, S.N. Zhou, L.L.P. Vrijmoed, Metabolites of mangrove endophytic fungus no.2534 from the South China Sea, Acta Sci. Nat. Univ. Sunyatseni 42 (2003) 52–54.
[20] N.C. Da Costa, M.Z. Chen, D. Merritt, L. Trinnaman, Methionine-containing cyclic dipeptides: Occurrence in natural products, synthesis, and sensory evaluation, in: ACS Symposium Series, Controlling Maillard Pathways to Generate Flavors, 1042, 2010, pp. 111–120.
[21] Y.-H. Chen, S.-E. Liou, C.-C. Chen, Two-step mass spectrometric approach for the identification of diketopiperazines in chicken essence, Eur. Food Res. Technol. 218 (2004) 589–597.
[22] N. Walchshofer, M.E. Sarciron, F. Garnier, P. Delatour, A.F. Petavy, J. Paris, Anthelmintic activity of 3,6-dibenzyl-2,5-dioxopiperazine, cyclo(L-Phe-L-Phe), Amino Acids 12 (1997) 41–47.
[23] N. Tsuruoka, Y. Beppu, H. Koda, N. Doe, H. Watanabe, K.A. Abe, DKP cyclo(L-Phe-L-Phe) found in chicken essence is a dual inhibitor of the serotonin transporter and acetylcholinesterase, PLoS One 7 (2012) e50824.
[24] H. Woehlecke, H. Osada, A. Herrmann, H. Lage, Reversal of breast cancer resistance protein-mediated drug resistance by tryprostatin A, Int. J. Cancer 107 (2003) 721–728.
[25] M. Maliepaard, G.L. Scheffer, I.F. Faneyte, M.A. van Gastelen, A.C. Pijnenborg, A.H. Schinkel, M.J. van De Vijver, R.J. Scheper, J.H. Schellens, Subcellular localization and distribution of the breast cancer resistance protein transporter in normal human tissues, Cancer Res 61 (2001) 3458–3464.
[26] N. Fani, E. Sattarinezhad, A. Bordbar, Identification of new 2,5-diketopiperazine derivatives as simultaneous effective inhibitors of ab-tubulin and BCRP proteins: Molecular docking, Structure-Activity Relationships and virtual consensus docking studies, J. Mol. Struct. 1137 (2017) 362–372.
[27] A.D. Borthwick, N.C. Da Costa, 2,5-Diketopiperazines in food and beverages: Taste and bioactivity, Crit. Rev. Food Sci. Nutr. 57 (2017) 718–742.
[28] X. Wang, Y. Li, X. Zhang, D. Lai, L. Zhou, Structural diversity and biological activities of the cyclodipeptides from fungi, Molecules 22 (2017) 2026.
[29] L.T.-H. Tan, K.-G. Chan, C.K. Chan, T.M. Khan, L.-H. Lee, B.-H. Goh, Antioxidative potential of a Streptomyces sp. MUM292 isolated from mangrove soil, BioMed Res. Int. 2018 (2018) 4823126.
[30] B.S. Thakkar, M. Albrigtsen, J.S. Svendsen, J.H. Andersen, R.A. Engh, Biofocussed chemoprospecting: An efficient approach for drug discovery, Chem. Biol. Drug Des. 90 (2017) 128–140.
[31] T. Furukawa, T. Akutagawa, H. Funatani, T. Uchida, Y. Hotta, M. Niwa, Y. Takaya, Cyclic dipeptides exhibit potency for scavenging radicals, Bioorg. Med. Chem. 20 (2012) 2002–2009.
[32] V. Rukachaisirikul, N. Khamthong, Y. Sukpondma, S. Phongpaichit, N.-p. Hutadilok-Towatana, P. Graidist, J. Sakayaroj, K. Kirtikara, Cyclohexene, diketopiperazine, lactone and phenol derivatives from the sea fan-derived fungi Nigrospora sp. PSU-F11 and PSU-F12, Arch. Pharm. Res. 33 (2010) 375–380.
[33] C.L.L. Chai, A.R. King, D.C.R. Hockless, cyclo-N-Acetyl-L-alanyl-N-methyl-L-alanyl (cyclo-N-Ac-L-Ala-N-Me-L-Ala), Acta Cryst C51 (1995) 1836–1838.
[34] P. Bouř, V. Sychrovský, P. Maloň, J. Hanzlíková, V. Baumruk, J. Pospíšek, M. Buděšínský, Conformation of the dipeptide cyclo(L-Pro-L-Pro) monitored by the nuclear magnetic resonance and Raman optical activity spectra. Experimental and ab initio computational study, J. Phys. Chem. A. 106 (2002) 7321–7327.
[35] M. Budesinsky, I. Cisarova, J. Podlaha, F. Borremans, J.C. Martins, M. Waroquier, E. Pauwels, Structures of cyclic dipeptides: An X-ray and computational study of cis- and trans-cyclo(Pip-Phe), cyclo(Pro-Phe) and their N-methyl derivatives, Acta Cryst B66 (2010) 662–677.
[36] M. Budesinsky, I. Cisarova, F. Borremans, J.C. Martins, E. Pauwels, Solid-state structure of cyclic dipeptides: An X-ray and computational study of cis- and trans-diketopiperazines of N-methyl-phenylalanine with the thia-pipecolic acids and thia-prolines, Acta Cryst B73 (2017) 1179–1193.
[37] B. Perić, N.P. Juraj, G. Szalontai, S.R. Veličković, F.M. Veljković, D. Vikić-Topić, S.I. Kirin, A crystallographic and solid-state NMR study of 1,4-disubstituted 2,5-diketopiperazines, J. Mol. Struct. 1234 (2021) 130157.
[38] L. Adler-Abramovich, D. Aronov, P. Beker, M. Yevnin, S. Stempler, L. Buzhansky, G. Rosenman, E Gazit, Self-assembled arrays of peptide nanotubes by vapour deposition, Nature Nanotechnology 4 (2009) 849–854.
[39] I. Alata, A. Pérez-Mellor, F. Ben Nasr, D. Scuderi, V. Steinmetz, F. Gobert, N.-E. Jaïdane, A. Zehnacker-Rentien, Does the residues chirality modify the conformation of a cyclodipeptide? Vibrational spectroscopy of protonated cyclodiphenylalanine in the gas phase, J. Phys. Chem. A 121 (2017) 7130–7138.
[40] I. Ianculov, R. Palicica, M. Butnariu, D. Dumbrava, I. Gergen, Achieving the crystalline state of chlorophyll of the Fir–tree (Abies alba) and the pine (Pinus sylvestris), Revista de chimie 56 (2005) 441–443.
[41] J.R. Deschamps, X-ray crystallography of chemical compounds, Life Sciences 86 (2010) 585–589.
[42] K.S. Etsè, F. Boschini, C. Karegeya, E. Roex, G. Zaragoza, A. Demonceau, R. Cloots, E. Mahmoud, Exploring organo-palladium(II) complexes as novel organometallic materials for Li-ion batteries, Electrochim. Acta 337 (2020) 135659.
[43] G.M. Sheldrick, SHELXT – Integrated space-group and crystal-structure determination, Acta Cryst. A71 (2015) 3–8.
[44] G.M. Sheldrick, Crystal structure refinement with SHELXL, Acta Cryst. C71 (2015) 3–8.
[45] G.M. Sheldrick, SADABS, Programs for Scaling and Correction of Area Detection Data, University of Gottingen, Gottingen, Germany, 1996.
[46] L.J. Farrugia, WinGX and ORTEP for Windows: an update, J. Appl. Cryst. 45 (2012) 849–854.

[47] P. Mahalakshmi, Vidyavathy Balraj, Priya Murugasen, G. Vinitha, V. Ragavendran, Synthesis, Structural-Spectral Characterization and Density Functional Theoretical Studies of Pyridine-4-carbohydrazide bis(4-hydroxynitrobenzene, J. Mol. Struct. (2021) 131362 (In press).
[48] M.J. Turner, J.J. McKinnon, S.K. Wolff, D.J. Grimwood, P.R. Spackman, D. Jayatilaka, M.A. Spackman, CrystalExplorer17, University of Western Australia, 2017.
[49] M.J. Frisch, G.W. Trucks, H.B. Schlegel, G.E. Scuseria, M.A. Robb, J.R. Cheeseman, G. Scalmani, V. Barone, B. Mennucci, G.A. Petersson, H. Nakatsuji, M. Caricato, X. Li, H.P. Hratchian, A.F. Izmaylov, J. Bloino, G. Zheng, J.L. Sonnenberg, M. Hada, M. Ehara, K. Toyota, R. Fukuda, J. Hasegawa, M. Ishida, T. Nakajima, Y. Honda, O. Kitao, H. Nakai, T. Vreven, J.A. Montgomery Jr., J.E. Peralta, F. Ogliaro, M. Bearpark, J.J. Heyd, E. Brothers, K.N. Kudin, V.N. Staroverov, R. Kobayashi, J. Normand, K. Raghavachari, A. Rendell, J.C. Burant, S.S. Iyengar, J. Tomasi, M. Cossi, N. Rega, J.M. Millam, M. Klene, J.E. Knox, J.B. Cross, V. Bakken, C. Adamo, J. Jaramillo, R. Gomperts, R.E. Stratmann, O. Yazyev, A.J. Austin, R. Cammi, C. Pomelli, J.W. Ochterski, R.L. Martin, K. Morokuma, V.G. Zakrzewski, G.A. Voth, P. Salvador, J.J. Dannenberg, S. Dapprich, A.D. Daniels, O. Farkas, J.B. Foresman, J.V. Ortiz, J. Cioslowski, D.J. Fox, Wallingford CT, Gaussian, Inc, 2009.
[50] T. Yanai, D.P. Tew, N.C. Handy, A new hybrid exchange-correlation functional using the Coulomb-attenuating method (CAM-B3LYP), Chem. Phys. Lett. 393 (2004) 51–57.
[51] R. Krishnan, J.S. Binkley, R. Seeger, J.A. Pople, Self-consistent molecular orbital methods. XX. A basis set for correlated wave functions, J. Chem. Phys. 72 (2008) 650–654.
[52] G.M. Morris, R. Huey, W. Lindstrom, M.F. Sanner, R.K. Belew, D.S. Goodsell, A.J. Olson, AutoDock4 and AutoDockTools4: automated docking with selective receptor flexibility, J. Comput. Chem. 30 (2009) 2785–2791.
[53] K.S. Etsè, G. Zaragoza, K.D. Etsè, Easy preparation of novel 3,3-dimethyl-3,4-dihydro-2H-1,2,4-benzothiadiazine 1,1-dioxide: molecular structure, Hirshfeld surface, NCI analyses and molecular docking on AMPA receptors, J. Mol. Struct. 1238 (2021) 130435.
[54] S.G. Aller, J. Yu, A. Ward, Y. Weng, S. Chittaboina, R. Zhuo, P.M. Harrell, Y.T. Trinh, Q. Zhang, I.L. Urbatsch, G. Chang, Structure of P-glycoprotein reveals a molecular basis for poly-specific drug binding, Science 323 (2009) 1718–1722.
[55] W.L. DeLano, PyMOL DeLanoScientific, 700, San Carlos, CA, 2002
[56] Z.P. Liang, J. Li, N-Methylphthalimide, Acta Cryst E62 (2006) o4274–o4275.
[57] J. Wan, B. Wu, Y. Pan, Novel one-step synthesis of 2-carbonyl/thiocarbonyl isoindolinones and mechanistic disclosure on the rearrangement reaction of o-phthalaldehyde with amide/thioamide analogs, Tetrahedron 63 (2007) 9338–9344.
[58] B.A. Burkett, C.L.L. Chai, D.C.R. Hockless, 1-Acetyl-4-[(1R, 2S, 5R)-3-menthyloxycarbonyl]piperazine-2, 5-dione, Acta Cryst C53 (1997) 327–329.
[59] D. Cremer, J.A. Pople, A general definition of ring puckering coordinates, J. Am. Chem. Soc. 97 (1975) 1354–1358.
[60] D. Cremer, On the correct usage of the Cremer-Pople puckering parameters as quantitative descriptors of ring shapes – a reply to recent criticism by Petit, Dillen and Geise, Acta Cryst B40 (1984) 498–500.
[61] A.P. Mendham, J. Spencer, B.Z. Chowdhry, T.J. Dines, M. Mujahid, A. Palmer, G.J. Tizzard, S.J. Coles, X-Ray crystallographic structure of the cyclic di-amino acid peptide: N,N'-diacetyl-cyclo(Gly-Gly), J. Chem. Crystallogr. 41 (2011) 1323–1327.
[62] M. Gdaniec, B. Liberek, Structure of cyclo(-L-phenylalanyl-L-phenylalanyl-), Acta Cryst. C42 (1986) 1343–1345.
[63] K.D. Kopple, D.H. Marr, Conformations of cyclic peptides. Folding of cyclic dipeptides containing an aromatic side chain, J. Am. Chem. Soc. 89 (1967) 6193–6200.
[64] K. Suguna, S. Ramakumar, K.D. Kopple, Structure of cyclo(-L-leucyl-L-tyrosyl-) monohydrate, C15H20N2O3.H2O, Acta Cryst C40 (1984) 2053–2056.
[65] K.S. Devi, P. Subramani, N. Sundaraganesan, M.S. Boobalan, D. Tamilvendane, Investigation on spectra (UV–Vis, vibrational, NMR, HRMS), electronic structure (DFT calculations), molecular docking and antidiabetic activity of N-((benzo[d]thiazol-2-ylthio)methyl)-N-cyclohexylcyclohexanamine – A Mannich base, J. Mol. Struct. 1219 (2020) 128604.
[66] P. Petrache, S. Rodino, M. Butu, G Pribac, M Pentea, M Butnariu, Polyacetylene and carotenes from Petroselinum sativum root, Dig. J. Nanomater. Bios. 9 (2014) 1523–1527.
[67] M. Pentea, M. Butu, I. Samfira, R.T. Cristina, M. Butnariu, Extraction and analytical study of salvinorin a from leaves of Salvia divinorum, Dig. J. Nanomater. Bios. 10 (2015) 291–297.
[68] I. Samfira, S. Rodino, P. Petrache, R.T. Cristina, M. Butu, M. Butnariu, Characterization and identity confirmation of essential oils by mid infrared absorption spectrophotometry, Dig. J. Nanomater. Bios. 10 (2015) 557–565.
[69] V. Krishnakumar, V. Balachandran, T. Chithambarathanu, Density functional theory study of the FT-IR spectra of phthalimide and N-bromophthalimide, Spectrochim. Acta A62 (2005) 918–925.
[70] R.M. Silverstein, G.C. Bassler, T.C. Morrill, Spectrometric Identification of Organic Compounds, 5th ed., Wiley, New York, USA, 1991.
[71] J.F. Malone, C.M. Murray, M.H. Charlton, R. Docherty, A.J. Lavery, X-H$\cdots\pi$ (phenyl) interactions. Theoretical and crystallographic observations, J. Chem. Soc., Faraday Trans. 93 (1997) 3429–3436.
[72] K. Coenen, F. Gallucci, B. Mezari, E. Hensen, M. van S. Annaland, An in-situ IR study on the adsorption of CO_2 and H_2O on hydrotalcites, Journal of CO_2 Utilization 24 (2018) 228–239.
[73] S. Ji, T. Jiang, K. Xu, S. Li, FTIR study of the adsorption of water on ultradispersed diamond powder surface, Applied Surface Science 133 (1998) 231–238.
[74] M.A. Spackman, D. Jayatilaka, Hirshfeld surface analysis, CrystEngComm 11 (2009) 19–32.
[75] K.S. Etsè, K.D. Etsè, P. Nyssen, A. Mouithys-Mickalad, Assessment of anti-inflammatory-like, antioxidant activities and molecular docking of three alkynyl-substituted 3-ylidene-dihydrobenzo[*d*]isothiazole1,1-dioxide derivatives, Chem.-Biol. Interact. 344 (2021) 109513.
[76] J.J. McKinnon, M.A. Spackman, A.S. Mitchell, Novel tools for visualizing and exploring intermolecular interactions in molecular crystals, Acta Cryst B60 (2004) 627–668.
[77] J.J. McKinnon, D. Jayatilaka, M.A. Spackman, Towards quantitative analysis of intermolecular interactions with Hirshfeld surfaces, Chem Commun (2007) 3814–3816.
[78] K.S. Etsè, G. Zaragoza, F. Boschini, A. Mahmoud, New N-methylimidazolium hexachloroantimonate: Synthesis, crystal structure, Hirshfeld surface and catalytic activity of in cyclopropanation of stryrene, Inorg. Chem. Commun. 122 (2020) 108291.
[79] K.S. Etsè, J. Dorosz, K.M. Christensen, J-Y. Thomas, I.B. Pop, E. Goffin, T. Colson, P. Lestage, L. Danober, B. Pirotte, J.S. Kastrup, P. Francotte, Development of Thiochroman Dioxide Analogues of Benzothiadiazine Dioxides as New Positive Allosteric Modulators of α–Amino-3-hydroxy-5-methyl-4-isoxazolepropionic Acid (AMPA) Receptors, ACS Chem. Neurosci. 12 (2021) 2679–2692.
[80] M.J. Turner, S.P. Thomas, M.W. Shi, D. Jayatilaka, M.A. Spackman, Energy frameworks: insights into interaction anisotropy and the mechanical properties of molecular crystals, Chem. Commun. 51 (2015) 3735–3738.
[81] C.F. Mackenzie, P.R. Spackman, D. Jayatilaka, M.A. Spackman, CrystalExplorer model energies and energy frameworks: extension to metal coordination compounds, organic salts, solvates and open-shell systems, IUCrJ 4 (2017) 575–587.
[82] K.S. Etsè, L. Comeron Lamela, G. Zaragoza, B. Pirotte, Synthesis, crystal structure, Hirshfeld surface and interaction energies analysis of 5-methyl-1,3- bis (3-nitrobenzyl)pyrimidine-2,4(1 H,3 H)-dione, Eur. J. Chem. 11 (2020) 91–99.